Monte Carlo calculations of coupled boson-fermion systems. II

D. J. Scalapino and R. L. Sugar
Institute for Theoretical Physics and Department of Physics, University of California, Santa Barbara, California 93106
(Received 15 June 1981)

We have recently developed a formalism for carrying out Monte Carlo calculations on systems with coupled boson-fermion degrees of freedom. Here we present the results obtained using these techniques on some specific systems. First the quantum-mechanics problem of a single boson coordinate linearly coupled to a fermion is studied. The fermion Green's function and the boson coordinate displacement are calculated and compared with exact results. Extending this analysis to a one-dimensional array, a field theory in one space and one imaginary time dimension is investigated. The fermion and boson Green's functions are calculated and compared with analytic results obtained in the limit where the bare boson frequency is much larger or much smaller than the characteristic fermion energies.

I. INTRODUCTION

We have recently proposed a method for carrying out Monte Carlo calculations for systems with both boson and fermion degrees of freedom.[1,2] Here we apply these techniques to some particular examples selected to illustrate the formalism and explore its utility. We find that our approach yields very accurate numerical results for lattice field theories in one space and one time dimension.

We begin by analyzing in some detail the quantum-mechanics problem of a boson linearly coupled to a fermion charge. The Euclidean action for this system is

$$S=\int_0^\beta d\tau\int dx\left[\tfrac{1}{2}M\left[\frac{\partial\phi(x,\tau)}{\partial\tau}\right]^2+\tfrac{1}{2}\kappa\phi(x,\tau)^2+\psi^\dagger(x,\tau)\left[\frac{\partial}{\partial\tau}-\frac{\partial^2}{\partial x^2}+\omega+\lambda\phi(x,\tau)\right]\psi(x,\tau)\right]. \tag{1.1}$$

Here, $\phi(\tau)$ and $\psi(\tau)$ are the boson and fermion fields, respectively. τ is the imaginary time and $\beta=1/kT$ is the inverse temperature. Physically, this action could represent a molecule whose important degrees of freedom correspond to a relative nuclear displacement and an electron orbital with the charge on the orbital linearly coupled to the nuclear displacement. When an electron is added to the orbital, the nuclear frame distorts lowering the energy of occupation from that of the undistorted configuration.

Next, we consider a field theory in one space and one imaginary time dimension with the action

$$S=\int_0^\beta d\tau\left[\tfrac{1}{2}M\left[\frac{\partial\phi(\tau)}{\partial\tau}\right]^2+\tfrac{1}{2}\kappa\phi(\tau)^2+\psi^\dagger(\tau)\left[\frac{\partial}{\partial\tau}+\omega+\lambda\phi(\tau)\right]\psi(\tau)\right]. \tag{1.2}$$

When this theory is placed on a spatial lattice with periodic boundary conditions, it describes a ring of molecules of the type described earlier, of coupled via a fermion transfer matrix element. Such a system has been previously introduced in discussions of polarons.[3] By adjusting the chemical potential ω so that there are many electrons on the ring, one goes over to the problem of one-dimensional electron-phonon systems and the possibility of a spontaneous Peierls lattice distortion in the ground state.[4]

In treating such systems it is natural to consider an adiabatic limit in which the nuclear rearrangement takes place on a time scale which is slow compared to the electronic motion. Formally, the opposite limit, in which the boson degrees of freedom respond rapidly compared to the fermion degrees of freedom, can also be considered. This lim-

it occurs when a Hubbard-Stratonovich[5] transformation is used to replace a four-fermion interaction by a bilinear fermion coupling to an auxiliary field. In this work, both limits will be investigated in order to test and interpret the Monte Carlo results.

By its nature a Monte Carlo procedure is like an experiment. One must make decisions regarding what is to be measured and then, once the results of the measurement are known, they must be interpreted. It turns out that solutions can be obtained for the two limiting cases in which the boson frequency $\Omega=(\kappa/M)^{1/2}$ is much less or much greater than the characteristic fermion frequency. We will often refer to these simply as the $M\to\infty$ or $M\to 0$ limit, with the idea of an oscillator with mass M and a fixed spring constant in mind. These limiting cases as well as the exactly soluble single-site problem provide a basis for interpreting the Monte Carlo results for the N-site problem. The single-site problem is discussed in Sec. II and the N-site problem is considered in Sec. III. In the Conclusion, Sec. IV, the question of the nature of the one-dimensional ground state and its dependence on the ratio of the boson to fermion characteristic response frequencies is raised. We also discuss further ideas for implementing Monte Carlo calculations of boson-fermion systems.

II. A QUANTUM-MECHANICS PROBLEM

In this section we consider a quantum-mechanics problem in which a harmonic oscillator is linearly coupled to a fermion charge. The Hamiltonian for this system can be written in the second quantized form

$$\tilde{H}=\Omega b^{\dagger}b+\omega c^{\dagger}c+\lambda x c^{\dagger}c, \tag{2.1}$$

where b and c are the destruction operators of the boson and fermion, respectively, $\Omega=(\kappa/M)^{1/2}$ and $x=(b+b^{\dagger})/(2M\Omega)^{1/2}$. The first term describes a relative displacement coordinate characterized by a mass M and a spring constant κ, the second term represents the fermion orbital energy, and the last term linearly couples the oscillator displacement to the fermion occupation. Physically, one can imagine a diatomic molecule to which we add an electron. In the presence of the added electron charge the relative displacement between the nuclei shifts. In this molecular interpretation it is natural to consider a Born-Oppenheimer picture in which the electron degree of freedom rapidly adjusts on a time scale set by ω^{-1} to the slower $\Omega^{-1}=\sqrt{M/\kappa}$ nuclear motion. This is the usual adiabatic limit and for fixed κ, $\Omega\to 0$ as $M\to\infty$. Here we will also be interested in the opposite limit, where ω/Ω is small or $M\to 0$. We will see that this corresponds to a Hubbard-Stratonovich formulation of a self-interacting fermion problem which for this particular case simplifies to a noninteracting problem because $c^{\dagger}cc^{\dagger}c=c^{\dagger}c$.

In the formalism that will be used, the natural quantities which appear are thermal Green's functions. In particular, the fermion and boson Green's functions which will be calculated are given by

$$G(\tau)=\langle T[c(\tau)c^{\dagger}(0)]\rangle \tag{2.2}$$

and

$$D(\tau)=\langle T[x(\tau)x(0)]\rangle, \tag{2.3}$$

with $c(\tau)=e^{\tilde{H}\tau}ce^{-\tilde{H}\tau}$ and $x(\tau)=e^{\tilde{H}\tau}xe^{-\tilde{H}\tau}$. Here, the averages correspond to a trace over $e^{-\beta\tilde{H}}/Z(\beta)$, with $Z(\beta)=\mathrm{Tr}e^{-\beta\tilde{H}}$. From the community relations one can show that G and D satisfy the well-known boundary conditions

$$G(-\tau)=-G(\beta-\tau), \tag{2.4}$$

$$D(-\tau)=D(\beta-\tau). \tag{2.5}$$

In our analysis it will be useful to keep in mind the behavior and meaning of these Green's functions which follow from expanding them in a complete set of energy eigenstates. For example, for $\tau>0$

$$G(\tau)=\sum_{n,m}\frac{e^{-\beta E_n}}{Z}|\langle m|c^{\dagger}|n\rangle|^2 e^{-\tau(E_m-E_n)}, \tag{2.6}$$

which at low temperatures becomes

$$G(\tau)\cong\sum_{m}|\langle m|c^{\dagger}|0\rangle|^2 e^{-\tau(E_m-E_0)}. \tag{2.7}$$

In this limit, the large τ behavior is determined by the lowest-lying excited state which couples to the ground state through $c^{\dagger}$. The Green's functions can also be thought of in terms of the Laplace transforms of certain types of power spectra. For example, the probability of adding an electron with energy ν to the molecule is given by the power spectrum

$$P(\nu)=\sum_{n,m}\frac{e^{-\beta E_n}}{Z}|\langle m|c^{\dagger}|n\rangle|^2\delta(\nu-(E_m-E_n)), \tag{2.8}$$

and the Laplace transform of this is just $G(\tau)$:

$$\int_0^\infty P(\nu)e^{-\nu\tau}d\nu=G(\tau). \tag{2.9}$$

Thus, the inverse Laplace transform of $G(\tau)$ is equal to the power spectrum Eq. (2.8) for adding a fermion to the system.

The Monte Carlo procedure which we will use has been developed in detail in Ref. 2. Here we provide a brief heuristic review before making use of it. To begin with, consider the partition function for the one-site system with the boson part expressed as a path integral, but the fermion part left as a trace over operators:

$$Z=\int \delta x(\tau)\exp\left[-\int_0^\beta d\tau\left[\frac{M}{2}\dot{x}^2(\tau)+\frac{\kappa}{2}x^2(\tau)\right]\right]\mathrm{Tr}T\exp\left[-\int_0^\beta d\tau[\omega+\lambda x(\tau)]c^\dagger c\right]. \tag{2.10}$$

Because the single-fermion Hamiltonian $H(\tau)=[\omega+\lambda x(\tau)]c^\dagger c$ commutes with itself at different times, the τ ordering symbol T is, in fact, unnecessary. However, in the N-site case in which $[H(\tau_1),H(\tau_2)]\neq 0$, it will be neccessary. Now it is straightforward to trace out over the fermions obtaining

$$Z=\int \delta x(\tau)\exp[-S_B(x(\tau))]\left[1+\exp\left[-\int_0^\beta d\tau[\omega+\lambda x(\tau)]\right]\right], \tag{2.11}$$

where $S_B(x(\tau))$ is the pure Bose action

$$\int_0^\beta d\tau[M\dot{x}(\tau^2)/2+\kappa x(\tau^2)/2].$$

If the T continuum is replaced by a lattice of L points $\tau_i=(i-\frac{1}{2})\Delta\tau$, and $i=1,2,\ldots,L$ and $L\Delta\tau=\beta$, then setting $x_i=x(\tau_i)$, Eq. (2.11) can be written in the discrete form

$$Z\cong\int\prod_{i=1}^L dx_i e^{-S_B(\{x_i\})}\left[1+\prod_{i=1}^L e^{-\Delta\tau(\omega+\lambda x_i)}\right]. \tag{2.12}$$

In this form we can proceed to carry out any of the usual Monte Carlo procedures using as an effective action

$$S_{\mathrm{eff}}(x_i)=S_B(\{x_i\})-\ln\left[1+\prod_{i=1}^L e^{-\Delta\tau(\omega+\lambda x_i)}\right]. \tag{2.13}$$

The fermion Green's function can be obtained in a similar manner with

$$G(\tau)=Z^{-1}\int \delta x(\tau)e^{-S_{\mathrm{eff}}(x(\tau))}\exp\left[-\int_0^\tau d\tau[\omega+\lambda x(\tau)]\right]\Big/\left[1+\exp\left[-\int_0^\beta d\tau[\omega+\lambda x(\tau)]\right]\right]. \tag{2.14}$$

On the discrete τ lattice this is just

$$G(\tau_j)=Z^{-1}\int\prod dx_i\exp[-S_{\mathrm{eff}}(\{x_i\})]\prod_{k=1}^j e^{-\Delta\tau(\omega+\lambda x_k)}\Big/\left[1+\prod_{k=1}^L e^{-\Delta\tau(\omega+\lambda x_k)}\right] \tag{2.15}$$

so that once the $\bar{N}$ Monte Carlo samples $\{x_i\}$ are obtained, $G(\tau_j)$ is

$$G(\tau_j)=\frac{1}{\bar{N}}\sum_{\{x_i\}}\left[\prod_{k=1}^j e^{-\Delta\tau(\omega+\lambda x_k)}\Big/\left[1+\prod_{k=1}^L e^{-\Delta\tau(\omega+\lambda x_k)}\right]\right]. \tag{2.16}$$

In Ref. 2, the following expression for the fermion lattice Green's function for the single-site problem was obtained:

$$G(\tau)=\left[1-f(\omega-\omega_B)\right]\exp\left[-(\omega-\omega_B)\tau+\frac{\omega_B}{\Omega''}(e^{-\tau\Omega}-1)-\frac{\omega_B}{\Omega''}(e^{-\tau\Omega}-1)(e^{\tau\Omega}-1)(e^{\beta\Omega}-1)^{-1}\right]. \tag{2.17}$$

Here $\Omega'=\sinh(\frac{1}{2}\Delta\tau\Omega)/(\Delta\tau/2)$, $\Omega''=\sinh(\Delta\tau\Omega)/\Delta\tau$, and $f(\omega)=(1+e^{\beta\omega})^{-1}$ is the usual Fermi function. The polaron binding energy ω_B is given by

$$\omega_B=\frac{\lambda^2}{2M\Omega'^2}. \tag{2.18}$$

The average displacement is given by

$$\langle x \rangle = -\frac{\lambda}{M\Omega'^2} f(\omega-\omega_B). \tag{2.19}$$

In the continuum limit $\Omega'=\Omega''=\Omega$ and $\omega_B=\lambda^2/2M\Omega^2=\lambda^2/2\kappa$. For this case, with $\omega-\omega_B>0$, the low-temperature large β ground-state limit of $G(\tau)$ is

$$G(\tau)=e^{-\omega\tau}e^{(\omega_B/\Omega)[\tau\Omega+(e^{-\tau\Omega}-1)]}. \tag{2.20}$$

Initially for $\tau\Omega<1$, G varies as $e^{-\omega\tau}$ but as $\tau\Omega$ exceeds one $G(\tau)$ varies as $e^{-(\omega_B/\Omega)}e^{-(\omega-\omega_B)\tau}$. Physically, this simply reflects the time scale Ω^{-1} for the boson degree of freedom to respond to the presence of a fermion. The factor $e^{-\omega_B/\Omega}$ is the well-known Franck-Condon overlap of the displaced ground-state oscillators. Taking the logarithm of G yields the two limiting forms

$$\ln G \sim \begin{cases} -\omega\tau, & 0<\tau<<\Omega^{-1} \\ -(\omega B/\Omega)-(\omega-\omega_B)\tau, & \Omega^{-1}<<\tau. \end{cases} \tag{2.21}$$

In our Monte Carlo calculations we proceeded through the lattice site by site. At the ith lattice site, a new value of the field was generated such that $x_i \to x_i+\Delta r$. Here, r is a random number between -1 and $+1$, and Δ is a parameter fixed so that roughly half the changes were accepted. Then the ratio of the actions was constructed:

$$e^{-[S_B(x_i+\Delta r)-S_B(x_i)]}\left[1+e^{-\Delta\tau\lambda\Delta r}\prod_{i=1}^{L}e^{-\Delta\tau(\omega+\lambda x_i)}\right]\Big/\left[1+\prod_{i=1}^{L}e^{-\Delta\tau(\omega\tau+\lambda x_i)}\right] \tag{2.22}$$

and, using the Metropolis algorithm, the change was accepted if this ratio was larger than a random number between zero and one.

Table I shows results from some typical Monte Carlo runs for $G(\tau)$ and $\langle x \rangle$, with $L=10$, $\beta=10$, $M=1.0$, $\omega=1.0$, $\Omega=0.5$, and $\lambda=0.5$. The column labeled "exact" gives the lattice results obtained for $G(\tau)$ and $\langle x \rangle$ from Eqs. (2.17) and (2.19). In each of the runs, the initial field configuration $\{x_i\}$ was set to zero and 100 warm-up sweeps of the lattice were made. With an acceptance ratio of 0.5 for changing a lattice coordinate an average sweep through ten lattice sites took $\sim$0.01 sec on the VAX we were using. The column labeled $[10^3,5]$ shows the results for $G(\tau)$ and $\langle x \rangle$ when 10^3 measurements were made, each separated by five sweeps of the lattice. σ gives the rms deviation. The $[10^3,10]$ column corresponds to 10^3 measurements, each separated by ten sweeps. Although it appears to have somewhat larger σ's for the larger τ values, a similar type of variation arises when the initial random-number seed is changed. We believe that the measurements for G are essentially uncorrelated for runs separated by five sweeps. The last two columns show the results of two runs starting with different random-number seeds with 10^4 measurements, each separated by five sweeps. While the fermion Green's function over a range of τ values agrees quite well with the exact lattice results, the value of $\langle x \rangle$ is small for this temperature and more difficult to determine. We found that by making a number of runs with different random-number seeds, reasonable results were obtained for $\langle x \rangle$. A plot of $\langle x \rangle$ versus temperature is shown in Fig. 1. The solid curve passes through the exact result given by Eq. (2.19). As kT increases, the average occupation of the fermion state approaches 0.5 and $-\langle x \rangle$ approaches one for $\lambda=0.5$, $M=1.0$, and $\Omega=0.5$.

Figure 2 shows the fermion Green's function $G(\tau)$ vs τ for an $L=30$ lattice, with $\omega=1.0$, $\Omega=0.5$, and $\lambda=1.0$. These results were taken using 100 warm-up sweeps through the lattice and 4000 measurements each separated by five sweeps. The smooth curve passes through the points of the exact lattice Green's function. While it is clear that there is good agreement between the Monte Carlo results and the exact results, it is difficult to interpret $G(\tau)$ in this form. However, from the general form of the spectral representation Eq. (2.7) and more particularly from Eq. (2.21), it is clear that a more interesting quantity to study is $\ln|G(\tau)/G(0)|$ shown in Fig. 3. In this figure the Monte Carlo data is shown as dots, and the dashed and solid lines correspond to the limiting short- and long-time behavior, respectively, given by Eq. (2.21). The data plotted in this form clearly show that the long-time behavior is dominated by an excitation of energy $\simeq$0.5 which is just equal to $\omega-\omega_B$ for the parameters of the run.

TABLE I. Monte Carlo results for $G(\tau)$ and $\langle x \rangle$ on a lattice of $L=10$ points, with $\beta=10$, $M=10$, $\omega=1.0$, $\Omega=0.5$, and $\lambda=0.5$. The exact results are listed in the last column of both tables for comparison. The bracket's notation is [number of measurements, lattice sweeps between measurements]. σ is the rms deviation computed for a given run. The lower two columns correspond to two runs which differ only in the initial random-number seed. The notation $a\ -b$ means $a\times10^{-b}$.

τ	$G[10^3,5]$	σ	$G[10^3,10]$	σ	Exact
0	0.9970	5.6 −04	0.9910	2.2 −03	0.9940
1	0.4127	4.1 −03	0.4128	4.1 −03	0.4129
2	0.1997	4.3 −03	0.2009	4.3 −03	0.1991
3	0.1060	3.8 −03	0.1080	3.9 −03	0.1054
4	5.914 −02	3.1 −03	6.190 −02	3.3 −03	5.933 −02
5	3.377 −02	2.3 −03	3.734 −02	2.8 −03	3.492 −02
6	1.956 −02	1.7 −03	2.384 −02	2.4 −03	2.138 −02
7	1.147 −02	1.3 −03	1.6275−02	2.1 −03	1.369 −02
8	6.872 −03	9.4 −04	1.207 −02	2.0 −03	9.321 −03
9	4.309 −03	7.0 −04	9.803 −03	2.0 −03	6.965 −03
$\langle x \rangle$	1.418 −02	2.0 −02	−1.74 −02	2.1 −02	−1.184 −02

τ	$G[10^4,5]$	σ	$G[10^4,5]$	σ	Exact
0	0.9945	5.0 −04	0.9936	5.6 −04	0.9940
1	0.4118	1.3 −03	0.4126	1.3 −03	0.4129
2	0.1979	1.3 −03	0.1986	1.3 −03	0.1991
3	0.1042	1.2 −03	0.1049	1.2 −03	0.1054
4	5.828 −02	1.0 −03	5.896 −02	1.0 −03	5.933 −02
5	3.402 −02	8.7 −04	3.475 −02	8.5 −04	3.492 −02
6	2.069 −02	7.2 −04	2.145 −02	7.1 −04	2.138 −02
7	1.314 −02	5.9 −04	1.393 −02	6.1 −04	1.369 −02
8	8.862 −03	5.1 −04	9.629 −03	5.3 −04	9.321 −03
9	6.523 −03	4.8 −04	7.271 −03	5.1 −04	6.965 −03
$\langle x \rangle$	−3.63 −03	6.3 −03	−1.313 −02	6.4 −03	−1.184 −02

The long-time behavior of $\ln[G(\tau)/G(0)]$ characterizes the bound polaron state while the short-time behavior gives the fermion energy in the undistorted molecular frame. The transient

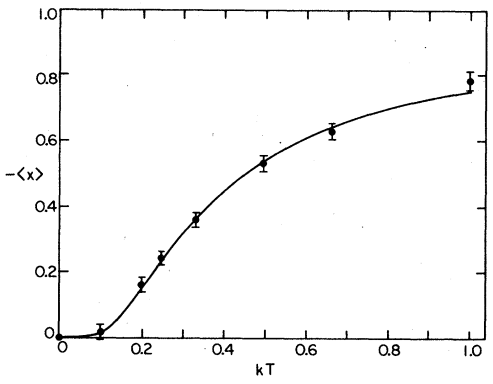

FIG. 1. Average displacement of the oscillator coordinate $\langle x \rangle$ versus temperature for $\omega-\omega_B>0$. The solid line is the exact result.

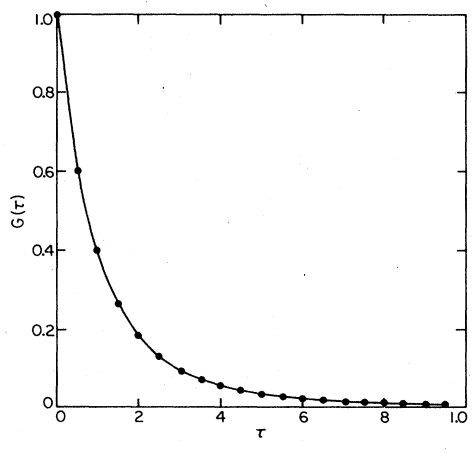

FIG. 2 Monte Carlo results for the fermion Green's function $G(\tau)$ vs τ for an $L=30$ site lattice, with $M=1.0$, $\omega=1.0$, $\Omega=0.5$, and $\lambda=1.0$ are shown as the dots. The solid curve is drawn through the points of the exact lattice Green's function for comparison.

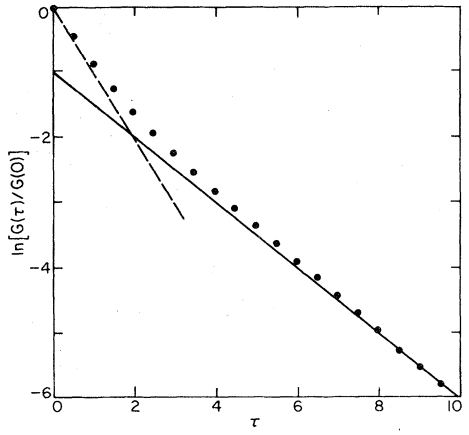

FIG. 3. $\ln[G(\tau)/G(0)]$ vs τ for the Monte Carlo data of Fig. 2. Note the crossover from $-\omega\tau$ (dashed line) when $\Omega\tau << 1$ to $-(\omega_B/\Omega)-(\omega-\omega_B)\tau$ (solid line) when $\Omega\tau >> 1$.

behavior associated with the crossover between the short- and long-time behavior of $G(\tau)$ has as a dynamic consequence the emission of bosons. This is most easily seen from the inverse Laplace transform of the low-temperature limit of $G(\tau)$, Eq. (2.20). As noted earlier, this gives the power spectrum for adding a fermion of energy ν:

$$P(\nu)=\int_{-i\infty}^{i\infty} e^{\nu\tau}G(\tau)\frac{d\tau}{2\pi}$$
$$=\sum\left[\frac{\omega_B}{\Omega}\right]^n\frac{1}{n!}e^{-(\omega_B/\Omega)}\delta((\omega-\omega_B+n\Omega)-\nu). \tag{2.23}$$

The allowed states have $\nu=\omega-\omega_B+n\Omega$, corresponding to a set of oscillator levels $n\Omega$ lying above the $\omega-\omega_B$ fermion state. The weight for exciting these states reflects the overlap of the ground state with these final states. In dealing with numerical data one can proceed by assuming a particular analytic structure for $G(\tau)$ or $P(\nu)$ and then fit the parameters in this form. We have not pursued this beyond seeing that the limiting slopes in Fig. 3 fit $-\omega$ and $-\omega+\omega_B$ given by Eq. (2.21).

III. THE TWO-DIMENSIONAL PROBLEM

In this section we consider the two-dimensional field theory whose action is given in Eq. (1.2). We introduce a spatial lattice with N sites and periodic boundary conditions. The system then corresponds to a ring of N molecules coupled by a nearest-neighbor fermion transfer interaction. The second quantized form of the Hamiltonian is

$$\tilde{H}=\sum_{n=1}^{N}[\Omega b_n^\dagger b_n+\omega c_n^\dagger c_n+\lambda x_n c_n^\dagger c_n$$
$$-t(c_{n+1}^\dagger c_n+c_n^\dagger c_{n+1})]. \tag{3.1}$$

The boson and fermion annihilation operators b_n and c_n are periodic, with $b_{N+1}=b_1$ and $c_{N+1}=c_1$. The field-displacement operator is related to $b_n^\dagger$ and b_n in the usual way, $x_n=(b_n^\dagger+b_n)/(2M\Omega)^{1/2}$ and $\Omega=(\kappa/M)^{1/2}$.

Just as before, it is useful to consider two limiting cases characterized by either a rapid or adiabatic response of the bosons to the fermions. Clearly, the adiabatic limit corresponds more nearly to the actual electron-phonon problem in the usual condensed matter systems. However, the rapid limit ($M\to 0$) is also of interest since it occurs whenever a four-fermion interaction is induced to a bilinear form by means of an auxiliary Hubbard-Stratonovich field.

The heuristic arguments of Sec. II can easily be extended to the N-site problem. In the absence of the boson field, the fermion Hamiltonian is

$$\tilde{K}=\sum_n[\omega c_n^\dagger c_n-t(c_{n+1}^\dagger c_n+c_n^\dagger c_{n+1})], \tag{3.2}$$

and its associated partition function has the well-known form

$$Z=\mathrm{Tr}e^{-\beta\tilde{K}}=\prod_k(1+e^{-\beta\epsilon_k}). \tag{3.3}$$

Here, $\epsilon_k=\omega-2t\cos k$ are the eigenvalues of an $N\times N$ matrix K which describes the single-particle motion

$$K_{mp}=\omega\delta_{mp}-t(\delta_{m,p+1}+\delta_{m,p-1}), \tag{3.4}$$

with δ defined modulo N so that the periodic boundary conditions of the ring are maintained. Using K, the partition function can be written as a determinant:

$$Z=\det(I+e^{-\beta K}), \tag{3.5}$$

where I is the $N\times N$ unit matrix.

Now, as in Sec. II, we will write the partition function for the combined fermion-boson system in a mixed form. Here the fermion operators are traced over, and the bosons are represented by a functional integral with the action

$$S_B=\int_0^\beta\sum_n\left[\frac{M\dot{x}_n^2(\tau)}{2}+\frac{\kappa}{2}x_n^2(\tau)\right]d\tau. \tag{3.6}$$

Tracing over the fermions gives

$$Z=\int\prod_n \delta x_n(\tau)e^{-S_B} \times\det\left[I+T\exp\left[-\int_0^\beta d\tau\, H(\tau)\right]\right], \quad (3.7)$$

where $H(\tau)$ is an $N\times N$ matrix $K+V(\tau)$, with

$$V(\tau)_{m,p}=\lambda x_m(\tau)\delta_{m,p}. \quad (3.8)$$

In going onto the τ lattice we note that

$$T\exp\left[-\int_{\tau_{i-1}}^{\tau_i} d\tau\, H(\tau)\right]=U_i+O(\Delta\tau^3), \quad (3.9)$$

where U_i has the form

$$U_i=e^{-K\Delta\tau/2}e^{-V(\tau_i)\Delta\tau}e^{-K\Delta\tau/2}. \quad (3.10)$$

Therefore, on the lattice

$$Z=\int\prod_{n,i}\delta x_n(\tau_i)e^{-S_B}\det(I+B_N\cdots B_1), \quad (3.11)$$

where $B_i=e^{-\Delta\tau K}e^{-\Delta\tau V(\tau_i)}$. Proceeding in the same manner it follows that the $N\times N$ matrix fermion Green's function is given by averaging

$$G(\tau_i-\tau_i')=B_i\cdots B_i'(I+B_{i-1}'\cdots B_1B_L\cdots B_i')^{-1}, \quad (3.12)$$

with the effective weight $e^{-S_B}\det(I+B_N\cdots B_1)$.

Equations (3.11) and (3.12) are just the forms derived previously in I.

In order to implement a Monte Carlo calculation using Eqs. (3.11) and (3.12) we proceeded as discussed in I. For a starting field configuration $\{x_n(\tau_i)\}$, which was actually taken to be zero, the fermion Green's-function equation (3.12) was determined. Then a sweep through the space-time lattice was begun, time slice by time slice. A change in a field element $x_n(\tau_i)\to x_n(\tau_i)+\Delta r$ was made, and the ratio of the fermion determinants was computed according to

$$R=1+[1-G_{nn}(\tau_i,\tau_i)](e^{-\Delta\tau\lambda\Delta r}-1), \quad (3.13)$$

with equal-time, n,n spatial element of Eq. (3.12) for the ith time slice

$$G(\tau_i,\tau_i)=(I+B_{i-1}\cdots B_1B_L\cdots B_i)^{-1}. \quad (3.14)$$

R was multiplied by the usual ratio of the boson part of the action, and if the result was larger than a random number between zero and one, the change in the field configuration was kept. If the change was kept, the equal-time Green's function was updated at every spatial point in the time slice τ_i according to

$$\bar{G}_{jk}(\tau_i,\tau_i)=G_{jk}(\tau_i,\tau_i)-\frac{[\delta_{jn}-G_{jn}(\tau_i,\tau_i)](e^{-\Delta\tau\lambda\Delta r}-1)G_{nk}(\tau_i,\tau_i)}{1-[1-G_{nn}(\tau_i,\tau_i)](e^{-\Delta\tau\lambda\Delta r}-1)}. \quad (3.15)$$

After passing through the ith time slice we go to the $(i+1)$th time slice with

$$G(\tau_{i+1},\tau_{i+1})=B_iG(\tau_i,\tau_i)B_i^{-1}. \quad (3.16)$$

When a measurement of $G(\tau_i,\tau_j)$ was to be made, we computed the expression given in Eq. (3.12) for the time slice we were on. Measurements were taken in such a way that all time slices were covered many times in a given run.

After a number of iterations, roundoff errors begin to accumulate in G. These could be eliminated by a fresh calculation of G starting from the given field configuration. However, we found it faster[6] to simply correct G by calculating δG, the deviation of G from its exact value:

$$\delta G=G-G(I+B_{i-1}\cdots B_1B_L\cdots B_i)G+O(\delta G^2). \quad (3.17)$$

The computer we were using carried 16 significant figures, so we implement this correction when approximately 8 figures had been lost due to roundoff errors.

To test this procedure, we studied the $M\to 0$ limit of the lattice model. In this limit it is straightforward to obtain the exact result by completing the square on x_n and integrating out the boson field separately at each site giving simply

$$(-\lambda^2/2\kappa)(c_n^\dagger c_n)^2=-\omega_B c_n^\dagger c_n .$$

This just shifts the chemical potential down by a factor ω_B. Then the remaining fermion problem is diagonalized by going to momentum space with the allowed k_n values equal to $2\pi n/N$, with $n=0$, $\pm1,\ldots,N/2$ for N even. The quasiparticle operators are $c_k^\dagger=(1/\sqrt{N})\sum_l e^{ikx_l}c_l^\dagger$ and their energies are just $\epsilon_k=-2t\cos k+\omega-\omega_B$. Taking the spatial Fourier transform of the fermion Green's function one obtains the free field result

$$G(k,\tau)=\langle c_k(\tau)c_k^\dagger\rangle=[1-f(\epsilon_k)]e^{-\epsilon_k\tau}.$$

The spatial Green's function is

$$G(n,\tau)=\frac{1}{N}\sum G(k,\tau)e^{ikn}. \tag{3.18}$$

Here we have simplified our notation for the space-time dependence of the average Green's function since it only depends on relative lattice space n and time $\tau=l\Delta\tau$ separations.

The Monte Carlo procedure was used to compute the fermion Green's function on a 10×10 space-time lattice. Typically, a run would consist of ten warm-up sweeps through the lattice and 1000 measurements, each separated by five complete sweeps. The resulting $G(n,\tau)$ data was then Fourier transformed to obtain $G(k,\tau)$. Several runs were made starting from different random-number seeds to check on the consistency of the rms errors. With an acceptance ratio of 0.5 for changing a site coordinate, an average time for sweeping through an $L=10$, $N=10$ lattice was several seconds on the VAX we were using. This was done for a variety of parameters and checked against the exact results. For $M=0$ our form of the action on a finite τ lattice gives the exact continuum limit. An interesting case is that of a half-filled band corresponding to $\omega=\omega_B$. Here we set $t=\lambda=1$ and $\kappa=2$ giving $\omega_B=0.25$. With $t=1$, the fermion bandwidth is four so that a value of $\beta=5$ ($kT=0.2$) gives a relatively degenerate Fermi sea, while a value of $\beta=1$ corresponds to a hot system. Figures 4(a) and 4(b) show the values of $\langle c_k^\dagger c_k\rangle$ vs k for $k=\pi/5l$, with $l=0,1,\ldots,5$ obtained from the Monte Carlo calculation. The exact values for a 10-site ring lay inside the dots and the solid line corresponds to $\langle c_k^\dagger c_k\rangle$ for an infinite ring.

In Fig. 5 the Monte Carlo result for the zero-time spatial Green's function $G(n,0)=\langle c_n c_1^\dagger\rangle$ is shown as the dots. Again the exact results for a 10-site lattice lay inside the dots. The solid line represents the zero temperature, $N\to\infty$ limit:

$$G(x)=\int_{-\pi}^{\pi}\frac{dk}{2\pi}e^{ikx}[1-f(\epsilon_k)]$$
$$=\frac{\sin\pi x-\sin\pi x/2}{\pi x}. \tag{3.19}$$

Clearly, for the half-filled finite ring $G(n,0)$ is an even function about $n=5$. It is remarkable how closely the finite-lattice result follows the $N=\infty$ behavior over the first five points. This clearly shows the Fermi-hole correlations.

Table II gives a comparison of the Monte Carlo calculations with the exact results for three k values for a run in which, ten warm-up sweeps of the 10×10 lattice were made followed by 1000 measurement sweeps. The first two k values correspond to k states which are occupied in the ground state. For $N=\infty$ the Fermi momentum k_F would be $\pi/2$. Thus, the equal-time value $G(k,0)=1-\langle c_k^\dagger c_k\rangle$ is small at low temperatures, where $\langle c_k^\dagger c_k\rangle$ is near unity. As τ increases, $G(k,\tau)$ grows since the excitation energy associated with the $k=0$ and $2\pi/5$ state is negative. For the half-filled band, the $k=3\pi/5$ state is unoccupied in the ground state leading to a value of $G(k,0)$ of order one at low temperatures. Since its energy is positive $G(k,\tau)$ decays with increasing τ.

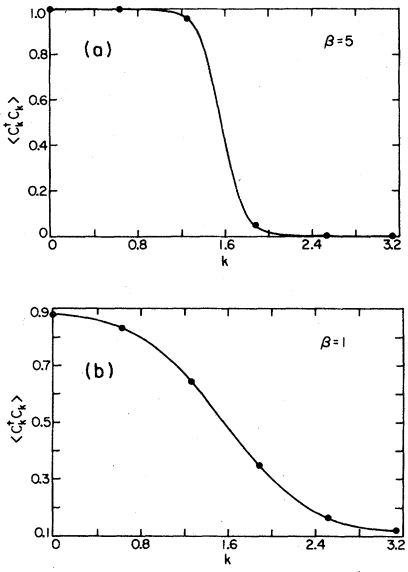

FIG. 4. MC results for the occupation number $\langle c_k^\dagger c_k\rangle$ for a ring of 10 sites, with $t=\lambda=1$ and $\kappa=2$. (a) is for $\beta=5$ and (b) is for $\beta=1$.

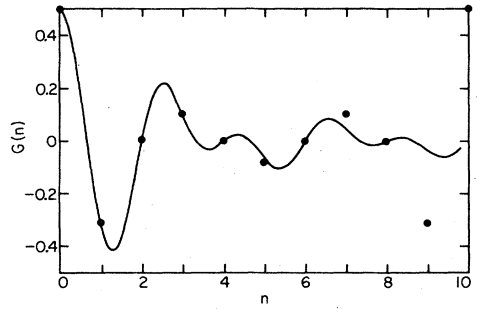

FIG. 5. Equal-time fermion Green's function G versus distance. The points are Monte Carlo data for a discrete lattice to ten sites which is half-filled and the solid curve is the continuum result. The ring G is naturally periodic while the continuum G decays.

TABLE II. Comparison of exact results for $G(k,\tau)$ with the Fourier transform of $G(n,\tau)$ obtained in a Monte Carlo run. Here the parameter values are $M=0$, $k=2$, $t=\lambda=1$, and $\omega=0.25$. The notation $a\ -b$ implies $a\times10^{-b}$.

	$k=0$		$k=2\pi/5$		$k=3\pi/5$	
τ	MC	Exact	MC	Exact	MC	Exact
0	4.709 −05	4.540 −05	4.253 −02	4.351 −01	0.9539	0.9565
1	1.488 −04	1.234 −04	5.759 −02	5.927 −02	0.7044	0.7022
2	2.249 −04	3.354 −04	7.838 −02	8.073 −02	0.5190	0.5155
3	7.718 −04	9.118 −04	0.1068	0.1100	0.3802	0.3785
4	2.383 −03	2.479 −03	0.1466	0.1498	0.2818	0.2779
5	6.705 −03	6.738 −03	0.2002	0.2040	0.2093	0.2040
6	1.829 −02	1.831 −02	0.2736	0.2779	0.1540	0.1498
7	4.965 −02	4.978 −02	0.3753	0.3785	0.1133	0.1100
8	0.1351	0.1353	0.5130	0.5155	8.349−02	8.073−02
9	0.3669	0.3679	0.6993	0.7022	6.162−02	5.927−02

In Fig. 6 we have plotted $\ln|G(k,\tau)/G(0,0)|$ vs τ for different momenta. As expected, the results correspond to straight lines with slopes proportional to $-\epsilon_k$. Results for ϵ_k vs k obtained from the slope of the lines in Fig. 6 are plotted in Fig. 7 along with a solid curve showing the exact result, $-2t\cos k$. The error bars lay inside the dots.

Turning next to the finite M calculations, it is of course straightforward to add the kinetic energy $\sum_i M\dot{x}_i^2/2$ of the oscillators to the Monte Carlo calculation. However, as in any experiment it is useful, in determining what to measure and how to interpret it, to have some general idea of the physical behavior of the system. For a vanishing transfer matrix element $t=0$, the N-site problem is, of course, equivalent to N separate one-site problems. In this case we have seen that if an electron is added to the site, the lattice will distort on a time scale set by Ω^{-1}. The coordinate $\langle x_i\rangle$ approaches $-\lambda/2\kappa$, and the fermion energy determining the decay of $G(\tau)$ changes from ω to $\omega-\omega_B$. Here we have assumed $\omega-\omega_B>0$ so that in the ground state the site is empty. Now, if the transfer term is present but $t<<\omega_B$, the initial response of the system is characterized by a narrow energy band $\omega-2t\cos k$. However, after a time of order Ω^{-1}, the lattice will distort and the behavior of $G(\tau)$ is determined by a small polaron band with energy $\omega-\omega_B$. The momentum eigenstates of this band will be a superposition of distorted single-site states, and the bandwidth will be exponentially narrower than $4t$ by a factor proportional to the Franck-Condon factor $e^{-(\omega_B/\Omega)}$. When the transfer coupling t is increased so that $t>>\omega_B$, the distortion extends over a number of sites of order $2t/\omega_B$, and its binding energy is reduced by a factor proportional to $\omega_B/2t$. This is the so-called large-polaron state.[3]

With the possibility of lattice distortions and extended structures it becomes more difficult to adequately cover the phase space. We found that it was useful to average over a number of runs which were started with different random-number seeds. Thus, typically we would gather data from 10 runs, each having 100 warmup sweeps and 100 measure-

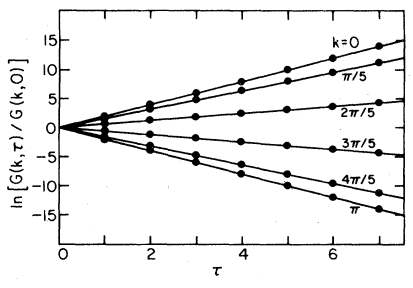

FIG. 6. MC results for $\ln|G(k,\tau_i)/G(k,0)|$ vs τ_i. The slopes give the energies of the various k states.

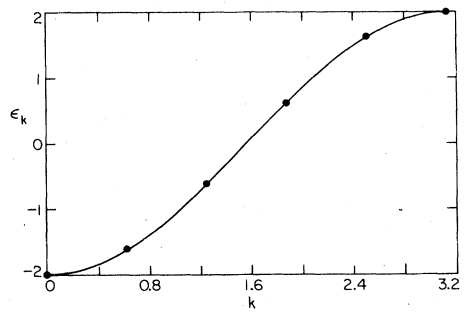

FIG. 7. ϵ_k vs k obtained from the slopes of ln$G$ for the 10-site ring. The solid line is $-2t\cos k$.

ment sweeps which were separated by five lattice sweeps. We also checked several different 10-run sequences to check that our errors were consistent.

We began by setting $t=0$ to see that the single-site results were satisfactorily reproduced. Then the transfer coupling t was increased and deviations of the type expected on the basis of the large-polaron theory were observed. However, it was as we began to decrese ω so that the system became degenerate that the most interesting behavior appeared.

Figure 8 shows the equal-time lattice-displacement-field correlation function

$$D(l)=\frac{1}{N}\sum_i \langle x_{i+l}x_i\rangle \tag{3.20}$$

determined from a Monte Carlo run on an $N=12$ by $L=10$ lattice. Here we have set $M=1$, $t=1$, $\Omega=0.5$, and $\lambda=0.75$. The chemical potential $\omega=1.125$ was adjusted until a half-filled band was obtained and β was set to ten corresponding to a low-temperature degenerate Fermi gas. The oscillating character of the displacement-displacement field correlations are clearly evident. A similar run on an $N=16$ by $L=10$ lattice is shown in Fig. 9.

The expectation value of $\langle c_k^\dagger c_k\rangle$ for the $N=12$, $L=10$ lattice at $\beta=10$ is shown in Fig. 10. The solid points with the error bars represent the results of various Monte Carlo runs taken with different starting random-number seeds. The solid curve passes through the points corresponding to a free-particle half-filled band, with $\beta=10$. The dashed curve is the result of the extreme adiabatic limit to be discussed below. There is a clear change in the occupation numbers in the ground

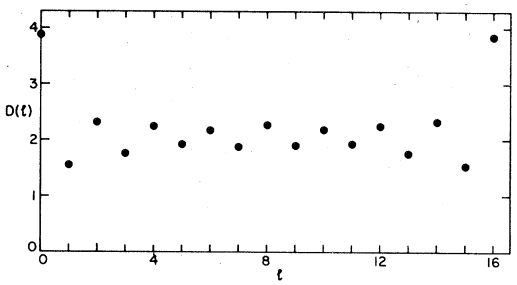

FIG. 9. Lattice-displacement-field correlation function $D(l)$ for a 16-site lattice.

state of the interacting system which smears the Fermi surface. Finally, Fig. 11 shows two plots of $\ln|G(k,\tau)/G(k,0)|$ for $k=\pi/2$ and $k=3\pi/2$. The Monte Carlo data is represented by the solid dots with the error bars. The dashed curve is simply a guideline. The solid curve is obtained from the extreme adiabatic limit discussed below. Clearly, these are qualitatively different from Fig. 6 for the $M=0$ case previously discussed.

In order to develop a framework with which to interpret this behavior, we consider the adiabatic limit in which M is sufficiently large that it is reasonable to proceed by neglecting the boson kinetic energy in $\tilde{H}$ in Eq. (3.1). Remember, as previously emphasized, this is just the opposite limit of neglecting the term $\sum M\dot{x}_i^2/2$ in the functional integral formulation. This latter case, the $M\to 0$ limit, corresponds to uncorrelated $x_n(\tau_i)x_n(\tau_j)$ fields, while the $M\to\infty$ limit corresponds to long-range τ correlation of $x_n(\tau_i)x_n(\tau_j)$. Dropping the lattice momentum terms of $\tilde{H}$ corresponds to the extreme adiabatic view in which a minimum energy (or free energy) state for the fermions is calcu-

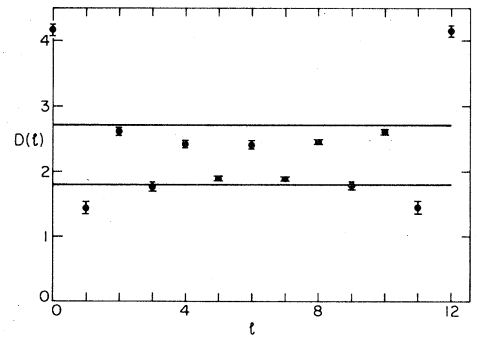

FIG. 8. Equal-time lattice-displacement-field correlation function $D(l)=(1/N)\sum_{n=1}^{N}\langle x_{n+l}x_n\rangle$ vs l for a 12-site lattice, with $M=1$, $t=1$, $\Omega=0.5$, $\lambda=0.75$, $\omega=1.125$, and $\beta=10$. In the extreme adiabatic limit $D(l)$ alternates between the values shown by the two solid lines.

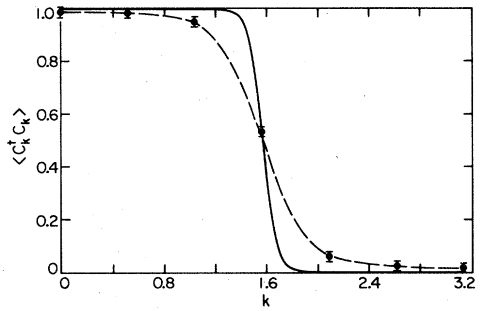

FIG. 10 Expectation value of $\langle c_k^\dagger c_k\rangle$ for the $N=12$ site lattice and the parameters listed in Fig. 8 are shown as the solid dots. The solid curve corresponds to what one would obtain for a noninteracting half-filled band, with $\beta=10$. The dashed line passes through the points which correspond to v_k^2, Eq. (3.26).

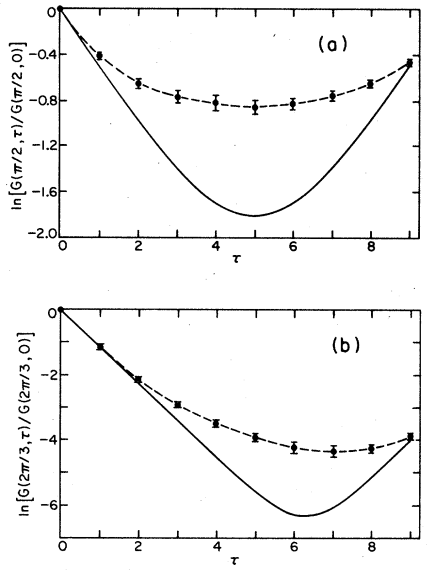

FIG. 11 $\ln|G(k,\tau)/G(k,0)|$ vs τ for the parameters listed in Fig. 8. (a) is for $k=\pi/2$ and (b) is for $k=3\pi/2$. The Monte Carlo data is represented by solid dots and the adiabatic result given by Eq. (3.29) is shown as the solid line. The dashed line through the Monte Carlo data is simply a guideline for comparison with the solid line.

lated for each possible lattice configuration specified by the x_n. Then the ground state is taken as the state which has the minimum possible energy (or free energy).

In the absence of the ion kinetic energy, the Hamiltonian is a quadratic form in the fermion operators and can therefore be numerically diagonalized for any configuration of the displacement field. To find the ground-state configuration one would seek the absolute minima of the energy over the parameter space $\{x_i\}$. The extended wave nature of the fermions introduces long-range couplings among the x_i coordinates, and the determination of the ground state is, in general, a nontrivial problem even though in the absence of the ion kinetic energy we are dealing with essentially a mean-field problem. Here we will consider a half-filled band with $N/4$ an integer. Such systems are expected to have a simple Peierls distortion.[7] To determine the parameters associated with this we note that in the $M\to\infty$ limit, Eq. (3.1) can be rewritten in the form

$$\tilde{H}=\sum_{n=1}^{N}\tfrac{1}{2}Kx_n^2+\omega c_n^\dagger c_n+\lambda x_n c_n^\dagger c_n - t(c_{n+1}^\dagger c_n+c_n^\dagger c_{n+1}). \tag{3.21}$$

Setting $x_n=x+(-1)^n\delta x$ in Eq. (3.21) and making the usual canonical transformation to the new quasiparticle creation operators for the conduction and valence bands

$$\gamma_k^{\dagger c,v}=u_k c_k^\dagger \pm v_k c_{k-\pi}^\dagger. \tag{3.22}$$

Here we take N to be an integer multiple of 4 so that $k=2\pi l/N$, with $l=0,\pm1,\ldots,N/4$ runs over the reduced zone. The resulting ground-state energy is

$$E_0=N\frac{\kappa x^2}{2}+\frac{\kappa N\Delta^2}{2\lambda^2}+\sum_k{}'\{\omega+\lambda x-[(2t\cos k)^2+\Delta^2]^{1/2}\}. \tag{3.23}$$

Here, $\Delta=\lambda\delta x$, and the prime denotes that the sum on k runs over the reduced zone. Minimizing E_0 with respect to x gives $x=-\lambda/2\kappa$ just as for the single-site case when the site has an average occupation of one-half. For a half-filled band, $\omega=-\lambda x$, which using the previous expression for x becomes $\omega=\lambda^2/2\kappa=\omega_B$. The resulting ground-state energy is

$$E_0=-\frac{N\omega_B}{4}+\frac{N\kappa\Delta^2}{2\lambda^2}\sum_k{}'[(2t\cos k)^2+\Delta^2]^{1/2}. \tag{3.24}$$

Minimizing E_0 with respect to Δ gives

$$1=\frac{2\omega_B}{N}\sum_k{}'\frac{1}{E_k}, \tag{3.25}$$

with $E_k=[(\epsilon_k)^2+\Delta^2]^{1/2}$ and $\epsilon_k=-2t\cos k$. Solving this numerically for $N=12$ leads to the results for Δ/t vs $t/2\omega_B$ shown in Table III.

TABLE III. Solution of the gap equation (3.25) for an $N=12$ site lattice.

Δ/t	$t/2\omega_B$	Δ/t	$t/2\omega_B$
0.05	1.971	0.55	0.429
0.10	1.137	0.60	0.413
0.15	0.858	0.65	0.398
0.20	0.717	0.70	0.384
0.25	0.632	0.75	0.372
0.30	0.573	0.80	0.360
0.35	0.531	0.85	0.350
0.40	0.498	0.90	0.340
0.45	0.471	0.95	0.331
0.50	0.449	1.00	0.322

The function v_k^2 is given by

$$v_k^2=\frac{1}{2}\left[1-\frac{\epsilon_k}{E_k}\right] \tag{3.26}$$

and $u_k^2=1-v_k^2$. In terms of the quasiparticle valence and conduction operators the Hamiltonian is

$$H=E_0+\sum_k E_k^c \gamma_k^{c\dagger}\gamma_k^c-\sum_k E_k^v \gamma_k^v \gamma_k^{v\dagger}, \tag{3.27}$$

with $E_k^c=E_k$ and $E_k^v=-E_k$ the conduction and valence quasiparticle energies, respectively. In the ground state the valence states are filled and the conduction states are empty.

Expressing the fermion operator $c_k^\dagger$ and c_k in terms of the conduction and valence quasiparticle operators we have

$$c_k^\dagger=u_k^\dagger \gamma_k^{c\dagger}+v_k\gamma_k^{v\dagger} \tag{3.28}$$

and its adjoint. Therefore

$$\begin{aligned}G(\tau)&=\langle c_k(\tau)c_k^\dagger(0)\rangle \\ &=u_k^2[1-f(E_k)]e^{-E_k\tau}+v_k^2 e^{E_k\tau}f(E_k)\,.\end{aligned} \tag{3.29}$$

Here the first term is the contribution associated with adding an electron to a conduction state k, while the second term corresponds to adding an electron to the valence state k. This latter situation can occur at finite temperature and is proportional to the thermal probability for finding a hole $[1-f(-E_k)]=f(E_k)$. At low temperatures $G_k(0)=u_k^2=1-v_k^2$ so that $\langle c_k^\dagger c_k\rangle=v_k^2$.

For the parameters associated with the Monte Carlo calculation on the $N=12$ lattice, $\omega_B=1.125$, which from Table III implies $\Delta\cong 0.5$. The dashed line in Fig. 10 passes through the values of v_k^2 appropriate to $\Delta=0.5$. Similarly in Fig. 11, the solid line is a plot of $\ln[G(k,\tau)/G(k,0)]$, with $G(k,\tau)$ given by Eq. (3.29) for an $N=12$ lattice, with $t=1$ and $\Delta=0.5$. Just as in the one-site case, we expect that the initial behavior for τ values less than Ω^{-1} reflects the dynamics of the added electron in the unrelaxed lattice configuration. The initial slope for

$$\ln[G(k=\pi/2,\tau)/G(k=\pi/2,0)]$$

is approximately -0.4, corresponding to a gap $\Delta=0.4$. At larger τ values, where $\tau\Omega\gtrsim 1$, the lattice will distort leading to the deviation of the Monte Carlo data from the $M=\infty$ adiabatic result. Whether this deviation reflects a bound polaronlike state or is simply a shift in Δ altering the entire band is not clear from our present measurements.

We can use these ideas to extract further spectral information from our Monte Carlo data. Naturally, this information will be model dependent. Specifically, suppose we assume that for short times $G(k,\tau)$ has the form given by Eq. (3.29). Then the energy spectrum associated with adding an electron in a given Bloch momentum state to the ground-state lattice configuration can be estimated from

$$-\{\ln[G(k,\Delta\tau)/G(k,0)]\}/\Delta\tau.$$

For k values equal to or greater than $\pi/2$, $G(k,0)=1-\langle c_k^\dagger c_k\rangle$ is sufficiently large that a reasonable estimate can be obtained from the Monte Carlo data. However, for values of k less than $\pi/2$, $G(k,0)$ becomes small and the accuracy of the data is not as high. Turning to the analytic model results, Eq. (3.29), we see that $\ln G(k,\tau)$ has a positive slope equal to E_k as τ goes to β. Now, although we have only data out to $\tau=\beta-\Delta\tau$, we know on general grounds that $G(k,\beta)=1-G(k,0)$. Thus we can estimate E_k for $k\leq\pi/2$ by computing

$$(\ln\{[1-G(k,0)]/G(k,\beta-\Delta\tau)\})/\Delta\tau.$$

In this way we obtained results for $k<\pi/2$. Combining the results for $k<\pi/2$ and $k\geq\pi/2$ gives the point shown in Fig. 12. For comparison the

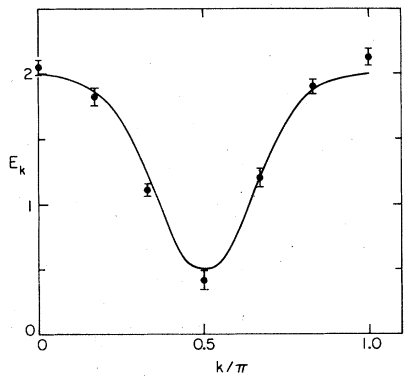

FIG. 12. "Energy spectrum" E_k of an added electron in the unrelaxed ground-state lattice configuration. The solid curve $E_k=[(2t\cos k)^2+\Delta^2]^{1/2}$, with $t=1$ and $\Delta=0.5$ is shown for comparison.

solid curve is $[(2t\cos k)^2+\Delta^2]^{1/2}$, with $t=1$ and $\Delta=0.5$.

Finally, we calculated x and δx for the parameters used in the $N=12$, $L=10$ model and found $x=-\lambda/2\Omega^2=-1.5$ and $\delta x=\Delta/\lambda=0.67$. For comparison, the measured values averaged over ten runs with different initial random-number seeds were $\langle x\rangle=-1.45$ and $\Delta=0.4$, giving $\delta x=0.53$. Using the extreme adiabatic results $x=1.5$ and $\delta x=0.67$ gave a lattice correlation function $D(l)$ which alternated between $[(x+\delta x)^2+(x-\delta x)^2]/2=2.7$ and and $(x=\delta x)\,(x-\delta x)=1.8$. These two limits are shown as solid lines in Fig. 8.

IV. CONCLUSION

We believe that we have demonstrated the utility of our approach for making Monte Carlo calculations of coupled boson-fermion systems in two dimensions. As is illustrated in the figures and tables we have obtained very accurate numerical results using a fairly small computer, a VAX-11-780, and a minimal amount of computer time. Typical running times for our program on a 10×10 lattice were one to two hours. We believe that we could study considerably larger two-dimensional systems by improving the efficiency of our computer codes or by using somewhat larger computers. Up to now we have focused our attention on the models defined in Eqs. (1.1) and (1.2) but there are a number of two-dimensional systems that are of interest in condensed matter and/or high-energy physics to which we plan to apply our methods.

It will be a challenging problem to extend our calculations to systems with more than one space dimension. Directly carrying over our techniques to higher dimensional systems would appear to be quite costly in terms of computer time. One approach which we plan to investigate is to generate the field configurations with an approximate determinant which can be calculated rapidly. If we denote by D_A and D the approximate and exact determinants, respectively, then the exact expection value of an operator A will be given by

$$\langle A\rangle=\langle AD/D_A\rangle_A/\langle D/D_A\rangle_A, \tag{4.1}$$

where $\langle\ \rangle_A$ means the expection value obtained from the field configurations generated with D_A.

For example, if the characteristic boson frequency is much less than that of the characteristic fermion response, one might take

$$D_A=\sum_\alpha\left[1+\exp\left[-\int_0^\beta d\tau E_\alpha(\tau)\right]\right]$$
$$\simeq\exp\left[-\int_0^\beta d\tau E_0(\tau)\right]. \tag{4.2}$$

Here, $E_0(\tau)$ is the ground-state energy for a fixed number of fermions in a frozen boson field $\{x_l(\tau)\}$ appropriate to the boson field configuration at time τ. This is the first term of an adiabatic expansion.[8] One can easily think of other ways of approximating the fermion determinant; however, this approach may be difficult to implement because of the exponential dependence of the determinant on the number of lattice points.

Returning to the model studied in this paper, a number of interesting questions remain for further investigation. For example, does the curvature for $\tau\Omega>1$ shown in Figs. 11(a) and 11(b) reflect a polaronlike state or rather an alteration of the gap Δ? In the zero-temperature limit, is there a critical value of the mass M (or Ω/t) below which the system has no gap or long-range lattice distortion but above which it does? Is there a critical value of λ where the simple Peierls distorted state is no longer the ground state?[7] Here we have seen for a finite ring that when $M=0$ there is no gap in the fermion spectrum and no long-range lattice displacement oscillations in $D(l)$. However, for M finite ($\Omega=0.5$), the $N=12$ and $N=16$ site spatial lattices show a gap in the fermion spectrum and structure in $D(l)$. At finite temperature, a spatially one-dimensional system of the type we are studying will not have long-range order. However, at zero temperature the quantum fluctuations may or may not destroy such order. It will be interesting to explore the way this depends upon M and the nature of the critical point. In addition, and perhaps as a probe of the M-critical problem, one would want to study the odd N lattices to see if solitons are present. It will also be important to examine the behavior of the two-particle Green's functions and, in particular, to see if a gap appears in their spectrum.

Beyond these questions, a number of transport problems in both the polaron and degenerate limits come to mind. Here the first question would be to explore ways of obtaining zero-frequency static transport coefficients as a function of temperature. Clearly, one would also want at the same time to gather thermodynamic data on the entropy and specific heat. An interesting challenge will be to

develop useful ways of extracting finite frequency transport coefficients from the imaginary time results. A simple example of this would be the reconstruction of an approximate power spectrum $P(\nu)$, Eq. (2.23) from the Monte Carlo data of Fig. 3.

ACKNOWLEDGEMENTS

We would like to thank S. Kivelson, J. R. Schrieffer, and W. P. Su for helpful discussions and comments. This work was supported by the National Science Foundation.

[1]D. J. Scalapino and R. L. Sugar, Phys. Rev. Lett. 46, 519 (1981).

[2]R. Blankenbecler, D. J. Scalapino, and R. L. Sugar, Phys. Rev. D 24, 2278 (1981). Hereafter referred to as I.

[3]T. Holstein, Ann. Phys. (Paris) 8, 325 (1959).

[4]In the continuum limit, the half-filled band is similar to the polyacetylene model discussed by W. P. Su, J. R. Schrieffer, and A. J. Heeger, Phys. Rev. Lett. 42, 1698 (1979); Phys. Rev. B 22, 2099 (1980).

[5]J. Hubbard, Phys. Rev. Lett. 3, 77 (1959); R. L. Stratonovich, Dokl. Akad. Nauk SSSR 115 (1957) [Sov. Phys.—Dokl. 2, 416 (1958).

[6]A similar procedure was used by A. Duncan and M. Furman (unpublished).

[7]Indeed for the $N=12$ lattice and the coupling constants we used the Peierls ground state which was obtained from a Monte Carlo minimization over $\{x_l\}$. It is not clear whether under other circumstances more exotic states may occur such as those obtained recently for the anisotropic next-nearest-neighbor interaction (ANNNI) model by P. Bak, Phys. Rev. Lett. 46, 791 (1981).

[8]Calculations of this type have been recently carried out by W. P. Su (private communication).